 doi:10.20944/preprints201809.0330.v1

Type of the Paper (Article). 96026190

Experimental and numerical comparison the velocity of elastic waves in nanofibers networks to mechanical characterization

Olivia Zurita[1]* and Margarita Navarrete[2]

[1] Insituto de Ingeniería, Universidad Nacional Autonoma de México, Mexico City; ozuritam@outlook.es
[2] Insituto de Ingeniería (Parque de Investigación e Innovación Tecnológica PIIT), Universidad Nacional Autonoma de México, Mexico, Nuevo Leon; mnm@pumas.iingen.unam.mx
* Correspondence: ozuritam@outlook.es; Tel.: +52 5524912536

Abstract: For development and successful application of any material, a clear understanding of their mechanical behavior is one of the most important things, but when it comes to nanofibers networks it become a challenge due to, their high porosity, many scales in their structure, and characteristics non-linear. Therefore, an experimental methodology in conjunction with a theoretical model that can fully consider their characteristics is still needed. In this work we proposed a model that incorporates the propagation of the elastic waves in two-phase media to determine the effective elastic modulus of electrospun membranes of PLA/gelatin given the mechanical properties of nanofibers, shape, distribution and concentration. The model was verified via laser ultrasonic testing. It was found that the values predicted for the effective modulus by the model were higher than the values obtained from experimental results. One explanation is due to the experimental density. As a result, the P-Wave velocity from the model best fit to experimental results and it has the same behavior, decrees as the concentration of gelatin in the solution. These results indicate the model and experimental methodology can assist in the dressing of nanofibers networks and electrospun materials.

Keywords: elastic properties; laser ultrasonic; mechanical behavior; fiber-network

1. Introduction

Porous scaffolds and electrospun membrane are commonly used in tissue engineering to reestablish the damaged tissues or organs to mimic the functions of native tissue [1]. It is important to note that scaffolds must have sufficient mechanical strength and stiffness to provide structural support to the growing tissue, as well as the suitable pore size, high surface to volume ratio, porosity and pore interconnectivity with the purpose of allowing the flow of nutrients, waste disposal, cellular communications and cell proliferation [2]. One of the most popular technologies to produce biomaterials is the electrospinning, because it allows controlling the structural parameters of the fibrous material such as the fiber orientation and diameter, texture and porosity [3,4]. To endure growth of biological tissue, a scaffold must be able to withstand and transfer local stresses uniformly over its total area. Further, it should be able to sustain forces arising from a large static pull of seeded live cells, loading spikes from the pulsating peripheral blood, dynamic load variations during a scaffold biodegradation as well as the progressively replaced by the extracellular matrix, etc [5].

The main approaches to determine the mechanical properties of fibers networks are: macro-testing according to ATSM D638 standard [6,7], mechanical testing on a single-strand nanofiber in axial strain [8,9] and recently the laser ultrasonic technique [10]. Nevertheless, when compare from these techniques the measurements over a single-fiber and material made of many fibers there are differences of three orders of magnitude [6]. The differences among them is due to the fact that the global mechanical response of a fiber network depends upon the specific fiber arrangement,

 doi:10.20944/preprints201809.0330.v1

interaction between neighboring fibers (e.g., contact adhesion, friction, etc) and the mechanical properties of the individual fibers [11]. So that, from a mechanical point view, the fiber networks do not fully fit the concept of bulk materials or thin films.

Currently with continuum micromechanics (effective medium) base on representative volume element, are been develop many models, such a Cox model, which was the first model to obtain the effective moduli of planar random fiber network [12]. Astom et al. and Wu et al, developed an effective constitutive relation for random planar fiber network by considering the strain energy dissipative for each individual fibers in a representative area element (RAE), [13–15], and more others models base on a volume averaging or homogenization[16–18]. Chetterjee extended the Astom et al and Wu et al work considering both isotropic and transversal isotropic fibers, [19–21].

Despite, the progress made in mechanical properties of the fiber networks, both the experiments and models on fiber networks remain a challenge and their utility, is limited by the absence of a theoretical framework with which to predict how the bulk mechanical properties depend on the properties of the individual fibers. Such a framework is inherently multiscale, with the membrane dimensions being on the centimeter length scale, while the underlying fibrillar architecture on the nanometer scale. Concerning this goal, there are only one application of the laser ultrasonic technique to measure the mechanical properties of fibers networks and anyone model to predict the elastic properties using the propagation of the elastics wave theory.

In this work, an approach to predict the velocity of propagation of a longitudinal wave that flies inside an electrospun membrane. In order to calculate its effective elastic modulus, we considering the material as a nano-porous with a fiber random distribution structure.

The longitudinal wave velocities are predicted using a micromechanical model in combination with Hashin and Strikman effective theory. The theoretical results are compared with our experimental results from measurements made in electrospun membranes with different concentration of polymeric solution using a laser ultrasonic technique, which has been widely used in medical area to evaluate the mechanical properties of skin [22,23] and soft material [24].

2. Materials and Methods

2.1 Materials

PLLA (Mw=192,787 g/mol) was purchased from Nature Works Gelatin (fish skin) and 1,1,1, 3,3,3-Hexafluoro-2-propanol (HFIP) was obtained from Sigma-Aldrich. For the purification was used Cloroform from Alfa Aesar A. Johnson Mathey Co. and Metanol from J.T. Baker.

2.2 Electrospinning

The PLLA and gelatin were dissolved in HFIP. After the two solutions were prepared, they were mixed together at different ratios 10/0, 9/1 and 8/2 (v/w) the overall concentration fixed at 13 % (w/v). The experimental setup included a high-voltage power supply (Spellman, USA) and digital controlled syringe pump (KD Scientific, USA). The electrospinnig process was in the following conditions: PLA membranes, the flow rate 1.0 ml /hr and positive voltage applied of 10 kV. At room temperature. PLA/gelatin membranes, the flow rate 0.5 ml /hr and positive voltage applied of 15 kV at room temperature. The electrosupun membranes were collected on a piece of aluminum foil placed at distance of 8 cm from the bunt tip of the capillary.

2.3 Morphological characterization

The average fiber diameter and volume of voids of the scaffolds were determined by analysis of SEM images. The scaffolds were cut into pieces of 0.5 x 0.5 cm and fixed with adhesive tape on aluminum sample pans, were sputter coated for 90 s with gold, ant tested using scanning electron microscope (SEM, Leica Cambridge Steroscan 440). Resultant images were imported into Image J software for analysis of fiber diameter, orientation and volume voids. The SEM images for PLLA-Gelatin illustrates a network of highly uniform and randomly oriented fibers, without the presence of beads defects.

Preprints (www.preprints.org) | NOT PEER-REVIEWED | Posted: 18 September 2018 doi:10.20944/preprints201809.0330.v1

2.4 Density determination

To approximate the experimental determination fo the density of the sample with different geometries is performed by the gravimetric method reported in [25,26], by measuring the thickness, width, and length of the samples.

Porosity was determined by finding the ratio of the measured density of the sample with the density of a bulk sample.

$$\varepsilon = 1 - \rho_{electrospun\ membrane} / \rho_{bulk\ sample}, \quad (1)$$

2.5 Laser ultrasonic testing

Laser ultrasonic is a non-contact technique that uses a short-pulsed laser to excite elastic waves that propagate within the material which velocity is dependent on the elastics and geometrical properties of the material [27].

Due to the morphology and fragility of the samples, for to apply the laser ultrasonic in these materials is necessary to have a specific conditioning, first one to have a material as a function of source ultrasonic, next to increase the amplitude of photoacoustic signal. Base on the work the Sherman [28], that found if we work in a ablative regime a large amplitude elastic stress waves are produced by the recoil momentum of the material ejected from the sample surface. Further enhancement of the stress wave amplitude can be obtained by confining the plasma with a transparent layer, such as water, polymer paint, or a glass film, through which a buried source is produced. Alternatively, a strong ablation source can be produced by explosive evaporation using an adsorbed layer covering the material surface so that not to damage the sample. Thus, to have a burned source we used like absorbed layer aluminum foil and a glass film. In this way, the samples are prepared so that the energy of the laser pulse, under ablative conditions, does not strike them directly. The waves are produced over aluminum foil and they are transfer to samples.

2.5.1 Sample preparation

Based on the experimental methodology used in [10]. To obtain the elastic moduli (K), electrospun membranes are tasted in the longitudinal, *L*, direction. See Figure 1. The samples are prepared with a cylindrical geometry, three samples for each gelatin concentration were evaluated.

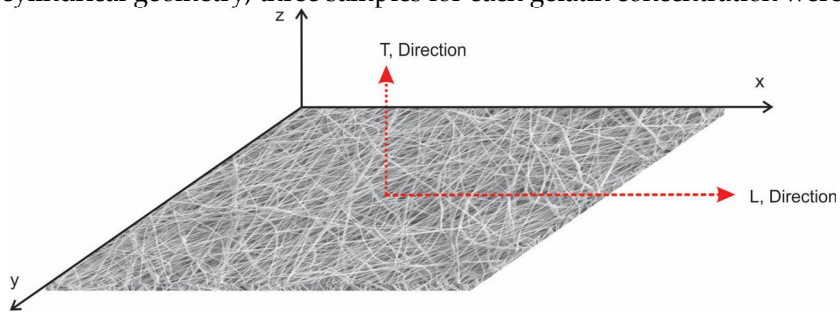

Figure 1. Schematic representation to the main directions over the electrosupun samples.

The membrane is wound into a cylindrical shape, wrapped in Maylar foil, and the placed inside the glass tube (inner diameter of 6 mm). A short metal rod, with the same diameter as that of the rolled membrane, are attached on each side of the cylindrical sample, taking care not to leave an air interface between the sample and metal road, as shown in Figure 2. This configuration is called, the cylindrical sample.

Preprints (www.preprints.org) | NOT PEER-REVIEWED | Posted: 18 September 2018 doi:10.20944/preprints201809.0330.v1

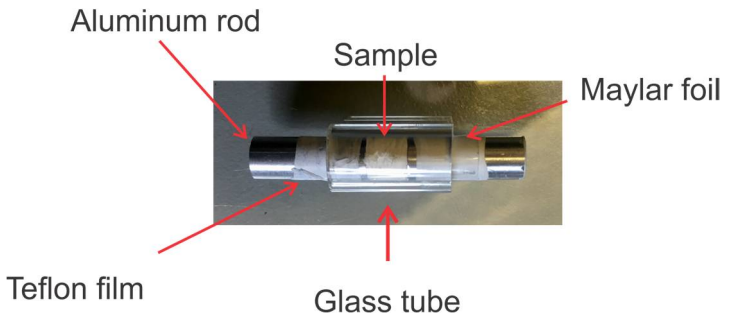

Figure 2. Picture from the cylindrical samples where is showed the materials that conform the sample holder.

2.5.2 System configuration

A schematic of laser ultrasonic setup is shown in a Figure 3. A source to stress wave generation used a Q-switched pulsed Neodymium Yttrium Aluminum Garnet (Nd:YAG) at 1064 nm with a pulse energy of 200 mJ and a Gaussian spatial distribution at 10 Hz rate repetition. The laser pulse width 6 ns with the spot diameter of 5 mm. The laser energy is absorbed by the aluminum in which takes places a generation of elastic waves, and travels through the sample. The generated elastic waves are detected on the other side of the sample with a piezoelectric PZT transducer (Olympus, V322), peak frequency 5 MHz, central frequency 4.80 MHz (broadband of 3.5 MHz). The signals are acquired and stored by a digitizing oscilloscope (Lecroy WaveRunner) with a bandwidth 1 GHz and sample rate 1 GS/s, triggered by a fast photodiode.

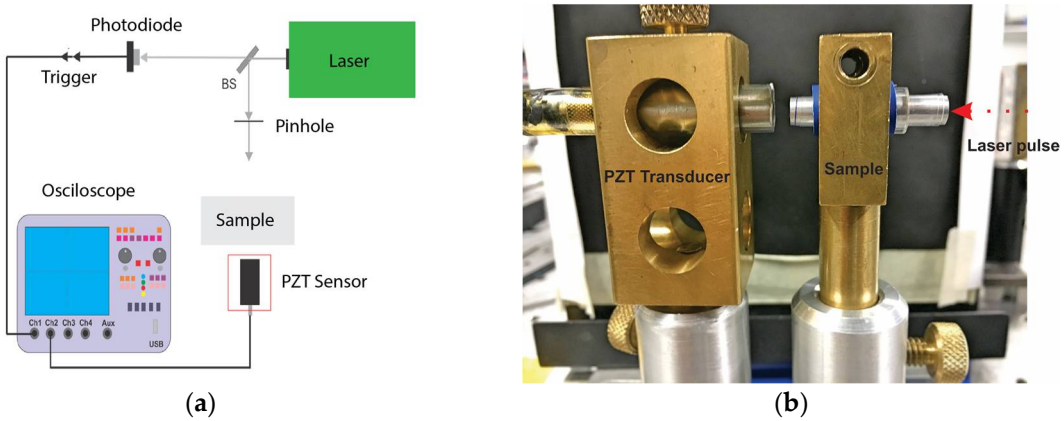

Figure 3. a) Representation of the experimental system configuration b) Picture taken of the experimental set up

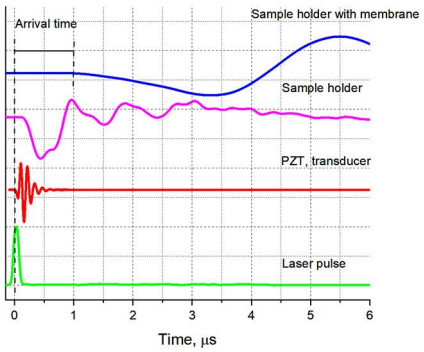

Figure 4. Arrival time signals i) signal the PZT sensor to a pulse of light laser ii) Signals of the arrival time with sample holder iii) Signals of the arrival time with sample holder and membrane. As we can see, the arrival time of the signals changes depending on the amount of materials in the way of the light pulse and the PZT sensor.

 doi:10.20944/preprints201809.0330.v1

149 2.5.3 Arrival time on the samples

150 Each one of the samples were fix in the way of the pulsed laser and the PZT sensor. We sent a
151 pulsed laser to sample and acquired the signal with a PZT transducer, five signals were acquired for
152 each sample. To calculate the average arrival time in electrospun sample we made a correction time.
153 It's means, the delay time produced by the materials that make up the sample holder was eliminated,
154 see Figure 4. The elastic modulus in the longitudinal direction was calculated from the arrival time
155 to P-Wave measured over the cylindrical samples using the dispersion of the elastic waves theory in
156 rods [29] (p.75).

157 **3. Experimental Results**

158 *3.1 Membrane characterization*

159 Using the methods described in the section 2.1 and the analysis of the SEM images of PLA/gelatin
160 fibers as is shown in Figure 5. The average diameter of each one of the samples are; to PLLA
161 nanofibers is 528.9 ±161 nm, to PLLA-Gelatin 10%, is 634 ±157 nm and PLLA-Gelatin 20% is 615 ± 130
162 nm. The density and percent porosity of the nine samples are shown in the Table 1, the density of
163 bulk material is fixed at 1270 Kg/m^3.

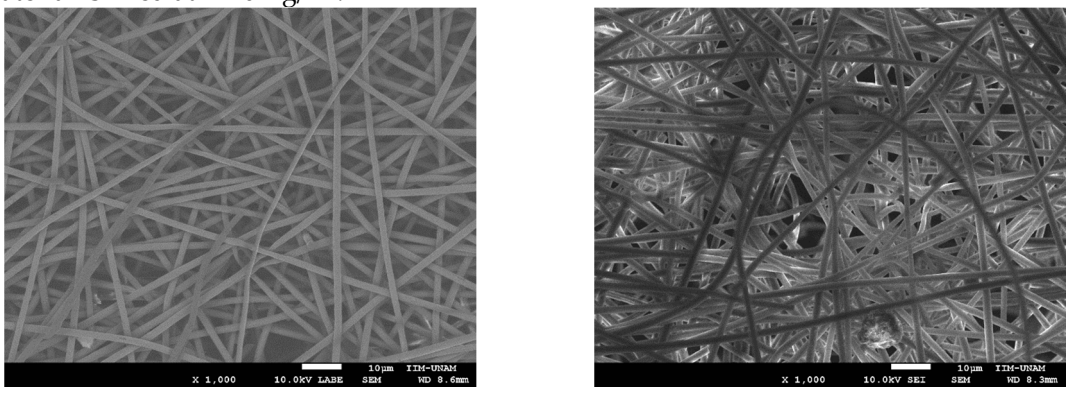

(**a**) (**b**)

164 **Figure 5.** Scanning electron micrograph of electrospun membranes: (**a**) PLA membranes using
165 the following conditions, applied voltage 10 kV, flow rate 1.0 ml/hr and working distance 8 cm; (**b**)
166 PLA/ fish skin gelatin membranes using the following conditions, applied voltage 15 kV, flow rate
167 0.5 ml/hr and working distance 8 cm.

168 **Table 1.** Morphological properties of the PLA/gelatin electrospun membranes. Density and porosity as a
169 function of the gelatin concentration.
170

Concentration PLA/gelatin (%wt)	Weight (gr)	Length (mm)	Volume (mm^3)	Density (kg/m^3)	Porosity (%)
10/0	21.86±0.09	4.13±0.13	101.7±13.3	214.9±28.9	0.82
10/0	25.20±0.10	4.36±0.02	107.4±2.5	234.7±6.4	0.81
10/0	16.76±0.11	3.80±0.08	93.7±7.5	178.9±15.6	0.85
9/1	13.66±0.15	3.57±0.07	87.9±5.8	155.4±12.1	0.87
9/1	13.40±0.07	3.30±0.06	81.2±5.1	165.0±11.1	0.86
9/1	15.18±0.11	3.42±0.16	84.2±13.3	180.3±29.8	0.85
8/2	14.20±0.12	3.57±0.24	87.9±21.4	161.5±40.8	0.86
8/2	13.80±0.07	3.48±0.08	85.8±6.7	160.9±13.4	0.86
8/2	12.92±0.08	3.44±0.22	84.8±18.5	152.3±34.2	0.87

171
172 Base on the methodology shown in the laser ultrasonic testing section the velocity of the P-Wave
173 and the elastic modulus calculated are displayed in the following Table 2.

Preprints (www.preprints.org) | NOT PEER-REVIEWED | Posted: 18 September 2018 doi:10.20944/preprints201809.0330.v1

Table 2. P-Wave velocity and elastic moduli of the PLA/gelatin electrospun membranes as a function of the gelatin concentration, density and porosity.

Concentration PLA/gelatin (%wt)	Density (Kg/m³)	Porosity (%)	Velocity (m/s)	Elastic Moduli (MPa)
10/0	214.9±28.9	0.82	442.8±37	42.1±0.0001
10/0	234.7±6.4	0.81	403.9±92	38.3±0.0002
10/0	178.9±15.6	0.85	412.7±169	30.5±0.0004
9/1	155.4±12.1	0.88	265.3±84	10.9±0.0002
9/1	165.0±11.1	0.87	270.4±31	12.1±0.0001
9/1	180.3±29.8	0.86	227.3±40	9.3±0.0001
8/2	161.5±40.8	0.87	258.2±52	12.0±0.0001
8/2	160.9±13.4	0.87	290.4±156	13.6±0.0003
8/2	152.3±34.2	0.88	262.0±37	10.9±0.0001

4 Theoretical approaching

The methodology to obtain the effective elastic modulus and P-Wave velocity of the fibers networks is shown in Figure 6. The mechanical properties of fibers network are determinate using the properties of single fibers and the microstructure of the fiber network (FN). A continuous the relation applied to obtain the mechanical properties of single fiber was developed.

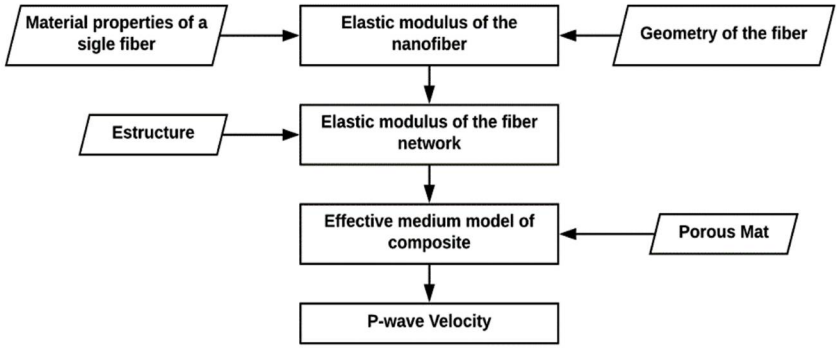

Figure 6. Procedure to calculate the P-Wave velocity, base on in a constitutive model.

As the fiber are made by a polymeric solution is necessary to obtain the average properties of fibers we assumed that they are isotropic and their density is obtained by a rule of mixtures [30]. The Poisson relation, and elastic modulus are obtained using the Voigt model.

$$\begin{aligned} \rho_f &= V_1\rho_1 + V_2\rho_2 \\ v_f &= V_1 v_1 + V_2 v_2 \\ E_f &= V_1 E_1 + V_2 E_2 \end{aligned} \tag{2}$$

4.1 Effective elastic modulus of the nanofiber.

According to [14,15], the elastic energies of deformation for individual fiber element of length l subject to such strain field are, stretching:$\pi\, E_f R^2 l\, \varepsilon_{zz}^2/2$, bending: $6\pi E R^4\left(\varepsilon_{zz}^2 + \varepsilon_{yz}^2\right)/l$ and shearing: $\pi E R^4\left(\varepsilon_{xz}^2 + \varepsilon_{yz}^2\right) l/\left(1 + v_f\right)$.

So that, the elastic energies under shearing and bending become equal for fiber segments of length $l = l_c = D, l_c = D/2\sqrt{6(1+v_f)}$. For long fiber segment with, $l \gg l_c$ the segment fiber is

Preprints (www.preprints.org) | NOT PEER-REVIEWED | Posted: 18 September 2018 doi:10.20944/preprints201809.0330.v1

assumed to deform only under bending and stretching. Then the effective elastic modulus to stretching and bending of a single fiber is given by [31,32].

$$E_{eff}^{strec} = E_f(1 + [\alpha_{stre}^2/D^2]), \quad (3)$$

$$E_{eff}^{ben} = E_f\left(1 + \left(\left[16/1 + v_f\right][\beta_{stre}^2/D^2]\right)\right), \quad (4)$$

where E_f is the elastic modulus of a single fiber , and α, β are length scale parameters.

4.2 Effective elastic modulus of the fiber network

The approach considers the following assumptions:

1. The fiber network structure is homogeneous structure
2. The fibers are straight and oriented in the same plane (Planar FN)
3. The fibers have identical length L_0 and diameter D
4. The fibers have randomly distribution
5. The space between the fibers is called void but is considered filled of air
6. The thickness and void space in the FN are uniform.
7. Due the high fiber content inside of volume membrane exist interaction between them, n_c.

Fiber networks are made of fibers with uniform lengths L_0 and uniformly distributed in the interval $[0, \theta_0], \psi(\theta, L)$ is in the form

$$\psi(\theta, L) = \delta(L - L_0)/\theta_0 \qquad (0 < \theta_0 < \pi), \quad (5)$$

where $\delta(L - L_0)$ is the Dirac function. For that distribution the mean number of contacts per fiber, can be estimated from [15].

$$n_c = \begin{cases} nL_0^2\{1 - \cos(\theta_0) + 2[\theta_0 + \sin(\theta_0)]r/L_0\}\theta_0\,, & 0 < \theta_0 \le \pi/2 \\ nL_0^2\{1 - \cos(\theta_0) + 2[2 + \theta_0 - \sin(\theta_0)]r/L_0\}\theta_0\,, & \pi/2 < \theta_0 \le \pi \end{cases}, \quad (6)$$

where n is the number of the fibers.

To a number of fibers above 500, the mean segment length can be estimated as [15]

$$\bar{l} = L_0/(n_c + 1), \quad (7)$$

The total number of nanofibers in a specific volume, is approximated with the excluded volume concept [33,34], considering that the elastic modulus of the fiber network is connected to the percolation threshold[20], the number of the fibers per unit volume at percolation q_p is inversely proportional to the excluded volume of one of the fibers.

$$q_p \cong 1/V_{ex} \quad (8)$$

If considered the fibers as spherical capped cylindrical tubes, of length L_0 and R. The exclude volume is given by Equation (9) where,θ is angle between two fibers (random distribution).

$$V_{ex} = \int_0^{\pi} \frac{32\pi}{3} R^3 \left[1 + \frac{3}{4}\left(\frac{L}{R}\right) + \frac{3}{8\pi}\langle\sin(\theta)\rangle\left(\frac{L}{R}\right)^2\right] d\theta \quad (9)$$

Number of the fibers inside a volume V is given by

$$q_p = n/V \quad (10)$$

To approximate the volume, V, occupied by the fibers in the total volume of samples with length L_x and L_y, (see Figure 7), we related the porosity of the fiber network using the Equation 11.

$$V_f = V_{sample}(1 - \phi_{voids}), \quad (11)$$

Preprints (www.preprints.org) | NOT PEER-REVIEWED | Posted: 18 September 2018 doi:10.20944/preprints201809.0330.v1

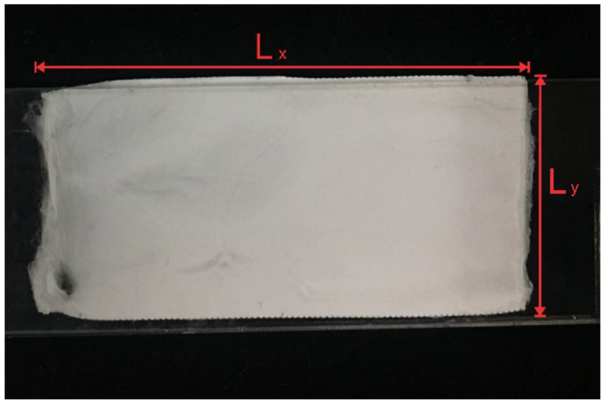

Figure 7. Photograph of PLA/gelatins samples where the red arrows represent their width and length using in the model.

where V_{sample} is the total volume of the samples, ϕ_{voids} the volume fraction of the space between the fibers (porosity) and V_{fibers} the volume occupied by the fibers. Since the fibers do not fill the entire volume of the sample, as we see in SEM images, a threshold is fix (that is function of the void spaces (porosity)), the threshold is a round 20 to 30 percent of the volume of sample. From the Equations (10) and (11) the number of the fibers in the sample is:

$$n = [V_{sample}(1 - \phi_{voids})]q_p, \quad (12)$$

According to Wang et al, [5] the total strain energy in x-direction adding the deformation of the fibers are considered, then the effective elastic modulus E_{eff} of the fiber network:

$$E_{eff} = f(n)\frac{3n\pi}{8\rho}\left[\frac{E_{eff}^{stre}}{4} + \frac{(2n-\pi)G}{3(2n+\pi)}g(z) + \frac{(4n^2-\pi^2)E_{eff}^{ben}}{4\pi^2\rho^2}\Gamma(0,z)\right], \quad (13)$$

where:

ρ= L_0/D, aspect ratio of nanofiber

G, Shear modulus of fiber

z = lc/l,

$g(z) = 1 - (exp - z)(z + 1)$,

Γ(0,z), incomplete gamma function,

$f(n) = 1 - (exp(1 - n/n_c)/2)$, the exponential decay function that describe the effect of the percolation threshold [13], n_c is the average number of contacts per fiber estimated with the Wu and Dzenis model [15]

4.3 Effective medium model of composite material

To predict the global mechanical behavior of the fiber network we applied a differential effective medium theory (DEM) considering the fiber networks as two-phase media [35,36], that consist of a matrix material (fiber network with a volume fraction, ϕ_{net}) with inclusion that are not connected (spaces between the fibers filled of air, which volume fraction is, ϕ_{voids}). We assume that the host material has a elastic moduli (K_m, μ_m) and the inclusion K_i. If we specify only the volume fractions of each one and the geometry of the inclusion we can predict the upper and lower bound to the mixture moduli by the relation of Hashin-Shtrikman-Walpole bounds for two constituents and considering that the spaces between the fibers are circular, the bounds are written as [37].

$$K^{HS\pm} = K_m + \frac{\phi_{voids}}{(K_m - K_i)^{-1} + \phi_{net}(K_m + \frac{4}{3}\mu_m)^{-1}}, \quad (14)$$

4.4 P-wave velocity

In order to obtain the P-wave V_p velocity, in the direction 1, we applied the Kuster and Toksoz (KT) model. In this model not consider the interaction between pores and applies the wave scattering theory and the classical theory of elasticity to spherical inclusions (ϕ_{voids}) dispersed in a continuous elastic matrix[38]. We considered a volume fraction of composites phases and their bulk modulus K^* [39,40]. The effective shear modulus vanishes because a two-phase medium cannot sustain any shear unless there be a solid continuum [38]. So that, the effective P-wave velocity is given by

Preprints (www.preprints.org) | NOT PEER-REVIEWED | Posted: 18 September 2018 doi:10.20944/preprints201809.0330.v1

$$V_p^* = \left[\frac{K^*}{\rho^*}\right]^{1/2}, \quad (15)$$

It must be emphasized that ρ^* is an effective density that changes as a function of the voids, , density of the air ρ_2, and density of the fiber ρ_1.

$$\rho^* = [\rho_1(1 - \phi_{voids}) + \rho_2\phi_{voids}, \quad (16)$$

5 Results

5.1 Comparison of the model to experimental measurements

The comparation of the experimental results with a theoretical model is showed in the Figure 8a where the P-Wave velocity decrease as a function of the gelatin concentration increase.

The experimental measurements of 10 and 20 wt% gelatin concentration samples, the P-Wave velocity is near to 250 m/s Figure 8b, by other side the samples made of PLA the velocity is over 400 m /s Figure 8c. In three kind of samples, the experimental values are within to the upper and lower bonds curves and they are in the same order of magnitude.

The membranes that contains different concentration of gelatin does not present a very large variation of velocity. As a result, the electrospun membrane made of PLA present a higher velocity and elastic modulus than the sample made of PLA/gelatin. The data suggest that the elastic modulus of membranes is sensitive to the gelatin solution concentration.

From a mechanical view the PLA/gelatin membranes have lower stiffness than made of PLA. That is to say the PLA/ gelatin samples shows a large deflection when they subjected to tension.

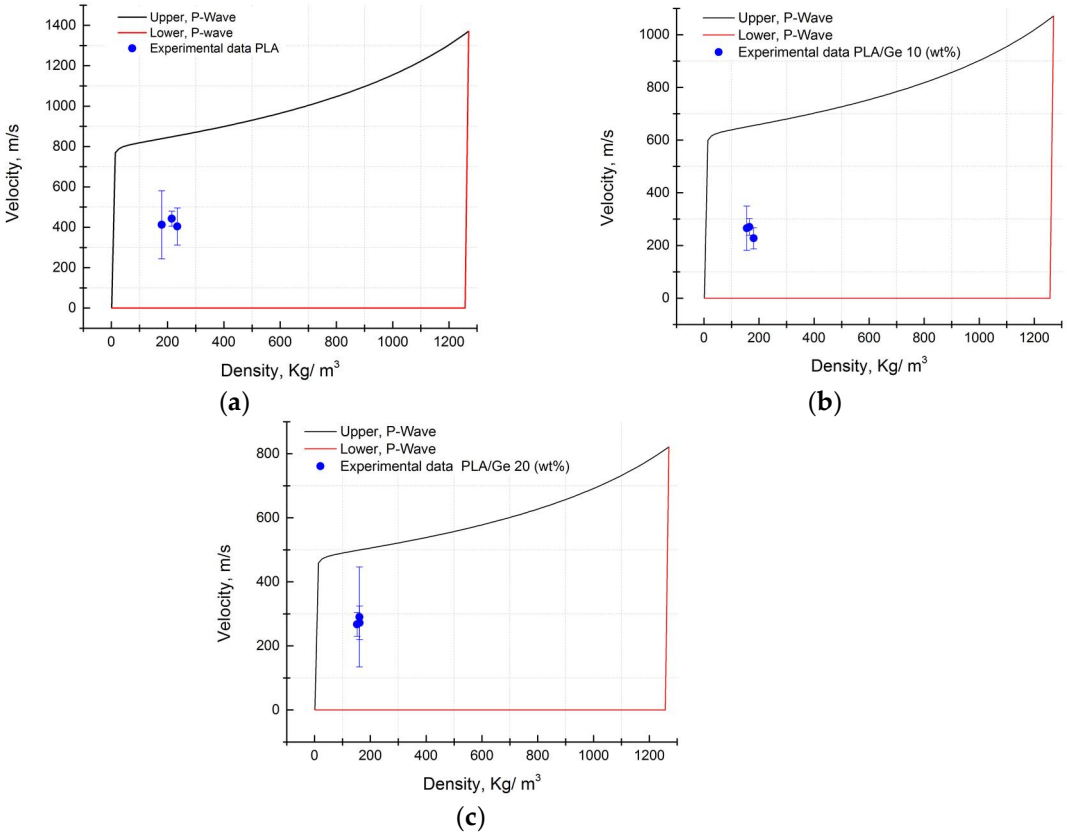

Figure 8. The P-Wave velocity (compresional) in a electrospun membranes as a function of the density. The solid curves are the upper and lower bonds predicted with Kuster and Toksoz (KT) model: (**a**) Correspond to PLA electrospun membrane; (**b**) correspond to PLA/ fish skin gelatin 10 % electrospun membrane; (c) correspond to PLA/ fish skin gelatin 20 % electrospun membrane.

In order to illustrate the comparison between theory and experiment the data are plotted in the Figure 9. The values of elastic modulus predicted are higher than the experimental results, the resultant best fit for the elastic modulus in PLA/gelatin samples to 10 and 20 % concentration, in both

Preprints (www.preprints.org) | NOT PEER-REVIEWED | Posted: 18 September 2018 doi:10.20944/preprints201809.0330.v1

cases are in the same order of magnitude, was found to be 160 MPa which is more than four times greater than modulus measured.

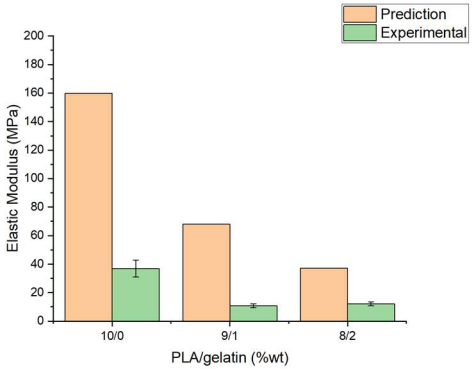

Figure 9. Mean elastic modulus of three kinds of electrospun membranes compared with the predictions generated by the model. A rise of the elastic modulus is observed as gelatin concentration decreases.

5 Discussion

The elastic modulus of electrospun membranes were calculated as function of gelatin concentration by arrival time of P-Waves. We compared the experimental results with a model integrated by a micromechanical model in combination with a model to propagation of the elastic waves in two-phase media. We use the combination of convectional models and results of tensile properties and SEM experiments.

The experimental results showed that the wave velocity is a function to the microstructural architecture and the discrepancies of the model in the elastic modulus revel limitation of the procedure experimental to measure the density of the samples. Even son the elastic moduli predicted and measured both are in the same order of magnitude, for the three polymeric mixtures. Therefore, it shows that the density has a great influence on the calculation in the elastic modulus but the agreement of the predictions of the model demonstrates experimentally that the properties of the electrospun membranes can be calculated and measured by the dispersion of elastic waves, using the methodology shown in this work. The next step is to develop theoretical framework that considers the fiber-network as a transversely elastic to approximate the S-Wave velocity. Which experimentally would allow us to measure 5 elastic constants instead of just one as is done so far.

5.1 Parametric analysis

All the assumptions of this model were originally developed for PLA-Gelatin fish skin fibers-network, with a random distribution, that presented cross-links and volume fraction of void in their interior of the network. But by varying different sample parameters, it easy to see the effect on the elastic P-wave velocity and the elastic modulus. Of observation Figure 10 is evident for the effect of the porosity in the velocity of the elastic waves that have consequence over the elastic modulus.

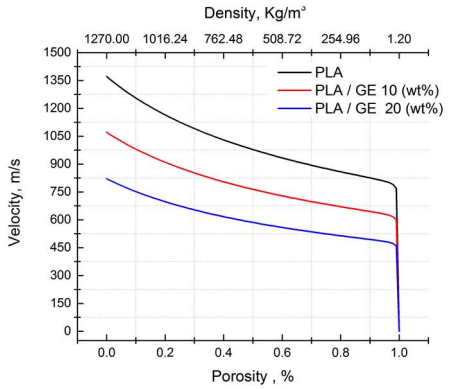

 doi:10.20944/preprints201809.0330.v1

319 **Figure 10.** P-Wave velocity in the PLA and PLA/ gelatin samples as a function of porosity
320 concentration and density

321 The attenuation of the P-wave velocity in longitudinal direction (draw direction) can be
322 predicted easily using the established model as long as the width to elastic modulus, aspect ratio, and
323 diameter of the fiber, concentration of the fibers and the porosity and volume of the sample specimen
324 are known.
325
326 **6 Conclusion**
327 This paper, we predicted the effective modulus of an electrospun membrane sheet with a
328 random distribution applying the laser ultrasonic technique to evaluate the mechanical properties of
329 electrospun materials instead the mechanical testing test. And the experimental results were
330 compared with theoretical framework that adopted advances previous efforts based on Reuss/Voight
331 elastic bounds, micromechanical models and effective medium approach, that results in a good
332 agreement with experimental results. Thus, this work provides a methodology to evaluate effective
333 elastic properties of nanofiber networks and electrospun membranes.
334
335
336

Acknowledgments: This work was supported by DGAPA-PAPIIT-UNAM under Grants IN105117 as well by II-UNAM under Grant 6593 and scholarship from CONACYT

References

1. Yan, S.; Xiaoqiang, L.; Shuiping, L.; Hongsheng, W.; Chuanglong, H. Fabrication and properties of PLLA-gelatin nanofibers by electrospinning. *J. Appl. Polym. Sci.* **2010**, *117*, 542–547, doi:10.1002/app.30973.
2. Cahill, S.; Lohfeld, S.; McHugh, P. E. Finite element predictions compared to experimental results for the effective modulus of bone tissue engineering scaffolds fabricated by selective laser sintering. *J. Mater. Sci. Mater. Med.* **2009**, *20*, 1255–1262, doi:10.1007/s10856-009-3693-5.
3. Wu, H.; Fan, J.; Chu, C. C.; Wu, J. Electrospinning of small diameter 3-D nanofibrous tubular scaffolds with controllable nanofiber orientations for vascular grafts. *J. Mater. Sci. Mater. Med.* **2010**, *21*, 3207–3215, doi:10.1007/s10856-010-4164-8.
4. Ayres, C. E.; Bowlin, G. L.; Pizinger, R.; Taylor, L. T.; Keen, C. A.; Simpson, D. G. Incremental changes in anisotropy induce incremental changes in the material properties of electrospun scaffolds. *Acta Biomater.* **2007**, *3*, 651–661, doi:10.1016/j.actbio.2007.02.010.
5. Wang, J.; Yuan, B.; Han, R. P. S. Modulus of elasticity of randomly and aligned polymeric scaffolds with fiber size dependency. *J. Mech. Behav. Biomed. Mater.* **2018**, *77*, 314–320, doi:10.1016/j.jmbbm.2017.09.016.
6. Croisier, F.; Duwez, A. S.; Jérôme, C.; Léonard, A. F.; Van Der Werf, K. O.; Dijkstra, P. J.; Bennink, M. L. Mechanical testing of electrospun PCL fibers. *Acta Biomater.* **2012**, *8*, 218–224, doi:10.1016/j.actbio.2011.08.015.
7. Thomas, V.; Jose, M. V.; Chowdhury, S.; Sullivan, J. F.; Dean, D. R.; Vohra, Y. K. Mechano-morphological studies of aligned nanofibrous scaffolds of polycaprolactone fabricated by electrospinning. *J. Biomater. Sci. Polym. Ed.* **2006**, *17*, 969–984, doi:10.1163/156856206778366022.
8. Tan, E. P. S.; Ng, S. Y.; Lim, C. T. Tensile testing of a single ultrafine polymeric fiber. *Biomaterials* **2005**, *26*, 1453–1456, doi:10.1016/j.biomaterials.2004.05.021.
9. Tan, E. P. S.; Lim, C. T. Novel approach to tensile testing of micro- and nanoscale fibers. *Rev. Sci. Instrum.* **2004**, *75*, 2581–2585, doi:10.1063/1.1775309.
10. Navarrete, M.; Vera-Graziano, R.; Maciel-Cerda, A.; Sánchez-Arévalo, F. M.; Godínez, F. A. Elastic Evaluation of Poly(Lactic Acid) Electrospun Membranes Using the Pulsed Photoacoustic Technique. *Int. J. Thermophys.* **2017**, *38*, 1–13, doi:10.1007/s10765-017-2251-5.
11. Wu, X.; Dzenis, Y. A. Collapse analysis of nanofibres. **2007**, doi:10.1088/0957-4484/18/28/285702.
12. Cox, H. L. The elasticity and strength of paper and other fibrous materials. *Br. J. Appl. Phys.* **1952**, *3*, 72–79, doi:10.1088/0508-3443/3/3/302.
13. Åström, J. A.; Mäkinen, J. P.; Alava, M. J.; Timonen, J. Elasticity of Poissonian fiber networks. *Phys. Rev. E* **2000**, *61*, 5550–5556, doi:10.1103/PhysRevE.61.5550.
14. Åström, J. A.; Mäkinen, J. P.; Hirvonen, H.; Timonen, J. Stiffness of compressed fiber mats. *J. Appl. Phys.* **2000**, *88*, 5056–5061, doi:10.1063/1.1315622.
15. Wu, X. F.; Dzenis, Y. A. Elasticity of planar fiber networks. *J. Appl. Phys.* **2005**, *98*, 093501, doi:10.1063/1.2123369.
16. Kouznetsova, V.; Brekelmans, W. A. M.; Baaijens, F. P. T. Approach to micro-macro modeling of heterogeneous materials. *Comput. Mech.* **2001**, *27*, 37–48, doi:10.1007/s004660000212.
17. Hill, R. Elastic properties of reinforced solids: Some theoretical principles. *J. Mech. Phys. Solids* **1963**, *11*,

357–372, doi:10.1016/0022-5096(63)90036-X.

18. Stylianopoulos, T.; Barocas, V. H. Volume-averaging theory for the study of the mechanics of collagen networks. *Comput. Methods Appl. Mech. Eng.* **2007**, *196*, 2981–2990, doi:10.1016/j.cma.2006.06.019.
19. Chatterjee, A. P. A model for the elastic moduli of three-dimensional fiber networks and nanocomposites. *J. Appl. Phys.* **2006**, *100*, 054302, doi:10.1063/1.2336088.
20. Chatterjee, A. P.; Prokhorova, D. A. An effective medium model for the elastic moduli of fiber networks and nanocomposites. *J. Appl. Phys.* **2007**, *101*, doi:10.1063/1.2732437.
21. Chatterjee, A. P. Modeling the elastic moduli of fiber networks and nanocomposites: Transversely isotropic filler particles. *J. Appl. Phys.* **2008**, *103*, 064316, doi:10.1063/1.2899961.
22. L'Etang, A.; Huang, Z. FE simulation of laser generated surface acoustic wave propagation in skin. *Ultrasonics* **2006**, *44*, 1243–1247, doi:10.1016/j.ultras.2006.05.077.
23. Li, C.; Huang, Z.; Wang, R. K. Elastic properties of soft tissue-mimicking phantoms assessed by combined use of laser ultrasonics and low coherence interferometry. *Opt. Express* **2011**, *19*, 10153, doi:10.1364/OE.19.010153.
24. Wang, H.-C.; Fleming, S.; Lee, Y.-C.; Law, S.; Swain, M.; Xue, J. Laser ultrasonic surface wave dispersion technique for non-destructive evaluation of human dental enamel. *Opt. Express* **2009**, *17*, 15592, doi:10.1364/OE.17.015592.
25. Loh, Q. L.; Choong, C. Three-Dimensional Scaffolds for Tissue Engineering Applications: Role of Porosity and Pore Size. *Tissue Eng. Part B Rev.* **2013**, *19*, 485–502, doi:10.1089/ten.teb.2012.0437.
26. Maspero, F. A.; Ruffieux, K.; Müller, B.; Wintermantel, E. Resorbable defect analog PLGA scaffolds using CO2 as solvent: Structural characterization. *J. Biomed. Mater. Res.* **2002**, *62*, 89–98, doi:10.1002/jbm.10212.
27. Scruby, C. B., Drain, L. E. *Laser Ultrasonics Techniques and Applications*; CRC Press, Ed.; 1990; ISBN 0750300507.
28. Sherman, B.; Liou, H. C.; Balogun, O. Thin film interface stresses produced by high amplitude laser generated surface acoustic waves. *J. Appl. Phys.* **2015**, *118*, doi:10.1063/1.4931937.
29. Graff, K. F. *Wave motion in elastic solids*; 1975; ISBN 9780486667454.
30. Voyiadjis, G. Z.; Kattan, P. I. *Mechanics of composite materials with MATLAB*; Springer, Berlin, Heidelberg, 2005; Vol. 1; ISBN 9783540243533.
31. Sun, L.; Han, R. P. S.; Wang, J.; Lim, C. T. Modeling the size-dependent elastic properties of polymeric nanofibers. *Nanotechnology* **2008**, *19*, 455706, doi:10.1088/0957-4484/19/45/455706.
32. Yuan, B.; Wang, J.; Han, R. P. S. Capturing tensile size-dependency in polymer nanofiber elasticity. *J. Mech. Behav. Biomed. Mater.* **2015**, *42*, 26–31, doi:10.1016/j.jmbbm.2014.11.003.
33. Balberg, I.; Anderson, C. H.; Alexander, S.; Wagner, N. Excluded volume and its relation to the onset of percolation. *Phys. Rev. B* **1984**, *30*, 3933–3943, doi:10.1103/PhysRevB.30.3933.
34. Berhan, L.; Sastry, A. M. Modeling percolation in high-aspect-ratio fiber systems. I. Soft-core versus hard-core models. *Phys. Rev. E - Stat. Nonlinear, Soft Matter Phys.* **2007**, *75*, 1–8, doi:10.1103/PhysRevE.75.041120.
35. Xu, S.; Payne, M. A. Modeling elastic properties in carbonate rocks. *Lead. Edge* **2009**, *28*, 66–74, doi:10.1190/1.3064148.
36. Li, H.; Zhang, J.; Shi, Y. Differential schemes for elastic properties of multiple-porosity rock. **2015**, 3305–3310, doi:10.1190/segam2015-5856193.1.
37. Mavko, G.; Mukerji, T.; Dvorkin, J. *The Rock Physics Handbook*; 2009; ISBN 9780511626753.

38. Kuster, G. T.; Toksöz, M. N. Velocity and attenuation of seismic waves in two-phase media: Part I. Theoretical formulations. *GEOPHYSICS* **1974**, *39*, 587–606, doi:10.1190/1.1440450.
39. Wang, Z.; Wang, R.; Weger, R. J.; Li, T.; Wang, F. Pore-scale modeling of elastic wave propagation in carbonate rocks. *GEOPHYSICS* **2015**, *80*, D51–D63, doi:10.1190/geo2014-0050.1.
40. Zhu, W.; Zhao, L.; Shan, R. Modeling effective elastic properties of digital rocks using a new dynamic stress-strain simulation method. **2017**, *82*, doi:10.1190/geo2016-0556.1.